minerals

MDPI

Article

Vermiculite Modified with Fe^{3+} Polyhydroxy Cations Is a Low-Cost and Highly Available Adsorbent for the Removal of Phosphate Ions

Fernando H. do Nascimento and Jorge C. Masini *

Departamento de Química Fundamental, Instituto de Química, Universidade de São Paulo, Av. Prof. Lineu Prestes 748, São Paulo 05508-000, Brazil

* Correspondence: jcmasini@iq.usp.br; Tel.: +55-11-3091-1469

Abstract: This paper demonstrates that intercalating Na^+ homoionic vermiculite with Fe^{3+} polyhydroxy cations (1:1 molar ratio OH^- to Fe^{3+}) significantly improved the affinity of the clay mineral-based sorbent toward phosphate. Kinetic experiments revealed that adsorption is fast, approaching an equilibrium within about 200 min of contact time, and that the rate-limiting step is the intra-particle diffusion. Adsorption isotherms fitted to the Freundlich equation and a two-site Langmuir model, consistent with the heterogeneity of adsorption sites. The separation factor derived from the Langmuir constant revealed that the adsorption was favorable and even irreversible for high-affinity minor adsorption sites. The adsorption capacity was 299 ± 63 μmol g^{-1} (9.3 ± 2.1 mg P g^{-1}), a value similar to several other clay-based phosphate adsorbents. Application to reservoir water spiked with 10 mg L^{-1} in P removed about 71% of the available phosphate.

Keywords: eutrophication; water treatment; adsorption; clay minerals; montmorillonite; bentonite; intercalation; cation exchange; oxyanions; adsorption capacity

Citation: do Nascimento, F.H.; Masini, J.C. Vermiculite Modified with Fe^{3+} Polyhydroxy Cations Is a Low-Cost and Highly Available Adsorbent for the Removal of Phosphate Ions. *Minerals* **2022**, *12*, 1033. https://doi.org/10.3390/min12081033

Academic Editors: Francisco Franco and Andrey G. Kalinichev

Received: 25 June 2022
Accepted: 5 August 2022
Published: 17 August 2022

1. Introduction

Phosphate is a limiting nutrient for microalgae growth in aquatic environments. A lack of phosphate in wastewaters, municipal wastes, and sewage sludges implies microalgae blooms that result in the severe eutrophication of water bodies [1]. For instance, phosphate concentrations as low as 1.12 μmol L^{-1} (0.11 mg L^{-1} PO_4^{3-}) may be related to phytoplankton blooms in Brazilian urban streams [1]. There is a quest to reduce phosphate emissions or develop materials that efficiently remove phosphate from wastewaters to prevent it from reaching lakes, rivers, and reservoirs [2–6].

Clay minerals are among the most studied potential adsorbents since they are environmentally compatible and abundant in nature [4,5,7–15] Vermiculite (Vt) is a 2:1 layered aluminosilicate that is known to afford high cation exchange capacity (CEC) since it has a permanent diffuse negative charge resulting from the isomorphic substitution of Si^{4+} by Al^{3+} in the tetrahedrons, and of Al^{3+} by Mg^{2+} in the octahedrons [16,17]. These permanent charges are counterbalanced by exchangeable cations such as Na^+, Ca^{2+}, and Mg^{2+}. The exchange of these simple cations by polynuclear cationic species of partially hydrolyzed Ti^{4+}, Zr^{4+} Al^{3+}, Fe^{3+}, and La^{3+} enhance the affinity of the modified clay minerals towards oxyanions such as phosphate [18,19], arsenate [20], and selenite [21].

For instance, modifying bentonites (a mixture of clay minerals containing 60% to 80% montmorillonite, Mt) with La^{3+} has been the basis for producing commercially available sorbents for phosphate (Phoslock®). The phosphate uptake occurs by forming $LaPO_4$, which precipitates on the surface of the clay support [10,12,22,23].

The retention of oxyanions onto Fe^{3+} polyhydroxy cations Mt and Vt may be explained by mixed mechanisms involving electrostatic interactions with the remaining positive charges on the partially hydrolyzed cations, or through a ligand exchange, as demonstrated

by the pH variations resulting from the adsorption [21,24,25]. Furthermore, the intercalation of polyhydroxy cations enhances the basal spacing, specific surface area, pore volume, and pore diameter of the clay minerals.

The main differences between Mt and Vt are their external specific surface areas (SSAs) which are determined by different methods using gas (N_2) or liquid (ethylene glycol monoethyl ether, EGME). While Mt affords an EGME SSA of up to 475 $m^2\ g^{-1}$ [26], Vt has 112 $m^2\ g^{-1}$ [21]. On the other hand, Vt has a CEC range of 80 to 126 $cmol_c\ kg^{-1}$ [24], whereas the CEC for Mt is between 60 and 150 $cmol_c\ kg^{-1}$ [22]. Another difference is that the basal spacing (d001) of Mt is systematically larger than that of Vt because its layer charge allows the separation between layers to occur at larger dimensions in an aqueous medium, producing materials with swelling properties [22].

Our research group studied Vt and Mt as adsorbents for aquatic pollutants removal [23,25,27–31]. In recent work, we studied phosphate removal by Na^+ homionic Mt prepared using its K10 commercial form before and after intercalation with Fe^{3+} polyhydroxy cations [19]. The present work demonstrates that intercalating Na^+ homoionic Vt with Fe^{3+} polyhydroxy cations is a simple process that results in an efficient adsorbent for phosphate anions with an adsorption capacity similar to several other materials, including Phoslock®, but using low-cost Fe^{3+} salts for the chemical modification.

2. Materials and Methods

2.1. Chemicals and Starting Materials

Analytical grade $FeCl_3$, NaOH, KH_2PO_4, and K_2HPO_4 were purchased from the Merck Group. All phosphate solutions were prepared from equimolar mixtures of KH_2PO_4 and K_2HPO_4 with a pH of around 6.9. The crude Vt sample from the Massapê mine (Paulistana, PI, Brazil) was milled with a mortar and pestle and sieved to select a granulometric fraction between 212 and 300 μm for the adsorption studies. The original vermiculite sample was crushed and extracted with 5% (*v*/*v*) HCl. The analysis of the extracts revealed that the leachable composition, expressed as a weight percent of their oxides, is Na_2O (0.0391 ± 0.001); K_2O (0.59 ± 0.02); CaO (2.16 ± 0.02); MgO (18.7 ± 0.2); Fe_2O_3 (4.75 ± 0.05); Al_2O_3 (8.34 ± 0.05); TiO_2 (1.29 ± 0.02); and BaO (0.104 ± 0.001) [32]. The vermiculite from Paulistana occurs as a hybrid basic rock with the following structural formula: $(Mg_{0.55}Ca_{0.03}Na_{0.01}K_{0.69})\ (Fe_{0.61}Ti_{0.13}Cr_{0.01}Mn_{0.01}Mg_{5.24})\ (Si_{6.1}Al_{1.67}Fe_{0.24})\ O_{20}OH_4.8H_2O$ [33].

2.2. Preparation and Characterization of the Adsorbents

Before modification with the Fe^{3+} polyhydroxy cations, the Na^+-exchanged Vt (Na-Vt) was obtained as previously described [31]. The Fe^{3+} polyhydroxy cations suspension was obtained by adding 50 mL of 0.40 mol L^{-1} NaOH to 50 mL of 0.40 mol L^{-1} $FeCl_3$ at the flow rate of 1.0 mL min^{-1} under vigorous stirring, providing a 1:1 molar ratio of OH^- to Fe^{3+}. The intercalation suspension was maintained at 50 °C for 48 h. After this incubation time, the intercalating suspension was pumped to the Na-Vt dispersion (heated at 50 °C) under vigorous stirring at 1.0 mL min^{-1} using a peristaltic pump. This procedure produced a ratio of 10 mmol of Fe^{3+} per gram of Na-Vt. Next, the suspensions were left standing for 72 h. The suspensions were centrifuged at 1000× *g* for 10 min in a Sorvall ST16R centrifuge (Thermo Fisher Scientific, Waltham, MA, USA), and the solid was washed five times with deionized water. Modified Vt was dried at 40 °C for 12 h under vacuum, crushed, and stored in a desiccator. It was named FeOH-Vt.

The basal spacing of Vt and FeOH-Vt was estimated by X-ray diffraction (XRD) in a Rigaku Miniflex instrument using Cu Kα radiation source at voltage = 30 kV, current = 15 mA, scattering slit = 4.2° and receiving slit = 0.3 mm. Continuous scan mode was used at scan speed = 1.000 min^{-1}, sampling width = 0.020°, and scan range from 2.0 to 50.000. Scanning Electron Microscopy (SEM) was conducted with a Fesem Jeol JSM-740 1 F instrument (Jeol Ltda, Tokyo, Japan).

The cation exchange capacity (CEC) of Na-Vt was determined by the exchange of sodium-saturated vermiculite with 1.0 mol L^{-1} ammonium acetate (pH 7.0) as described in [34]. The released Na^+ was quantified by flame photometry.

2.3. Adsorption Studies

Adsorption experiments used a thermostatic (25.0 ± 0.5 °C) orbital shaker at the stirring rate of 250 r.p.m. All the adsorption experiments were conducted in polypropylene centrifuge tubes from Corning® (capacity of 15 mL), horizontally accommodated inside the shaker. Dispersions were centrifuged at 4000× *g* for 15 min and filtered through 0.45-µm syringe filters (hydrophilic Minisart®, Sartorius Stedim Biotech GmbH, Germany).

The effect of the adsorbent dose evaluated the adsorption of 10.0 mL of 4.84 × 10^2 µmol L^{-1} (15 mg L^{-1} in P) phosphate buffer (pH 6.9) onto 25.0, 50.0, 75.0, and 100 mg of adsorbent dispersed in 10.0 mL of deionized water. The contact times were 200 min (data available in Table S1).

Kinetic curves were obtained by dispersing 2.0 g of FeOH-Vt in 200 mL of 4.84 × 10^2 µmol L^{-1} phosphate solution in a 500 mL beaker. The dispersion was continuously stirred in the orbital shaker, and small dispersion aliquots (1 mL) were sampled after 5, 10, 20, 40, 80, 120, 160, 200, 240, 280, 320, and 360 min of contact time (data available in Table S2). The dispersions were then quickly filtered through 0.45-µm syringe filters, and the solutions were stored at 4 °C until the determination of the free phosphate concentrations.

Adsorption isotherms (25.0 ± 0.5 °C) were constructed by adopting 200 min of contact time, using 100 mg of adsorbent dispersed in phosphate solutions (10.0 mL, pH 6.9), with the initial concentrations varying from 32.3 to 8.07 × 10^3 µmol L^{-1} (1.0–250 mg L^{-1} in P). The dispersions were centrifuged at 4000× *g*, and the supernatants were carefully separated, avoiding resuspension of the centrifuged adsorbent. The supernatants were filtered through syringe filters and stored in the refrigerator (4 °C) until the analysis (data available in Table S3).

The spectrophotometric determination of the free phosphate concentrations was based on their reaction with ammonium molybdenum (2.5 × 10^{-3} mol L^{-1} in 0.20 mol L^{-1} HNO_3) followed by the reduction of Mo(VI) to Mo(V) by 5.0% (m v^{-1}) ascorbic acid in the presence of 100 mg L^{-1} Sb as a catalyst [35]. Absorbance measurements were made in an Ocean Optics USB4000 spectrometer (Ocean Insight, Rochester, NY, USA) with an LS-1-LL tungsten halogen light source, connected by two optical fibers (600 µm diameter, 1 m long) to a 1 cm pathlength flow cell.

2.4. Computation

The adsorbed amount of phosphate (q) was computed as:

$$q = \frac{(C_{P,i} - C_P)V}{m} \quad (1)$$

where $c_{P,i}$ is the initial concentration of phosphate (in µmol L^{-1}), c_{P-} is the free concentration after a given contact time with the adsorbent, V is the volume of solution where the adsorbents were dispersed (10.0 mL), and m is the mass of the adsorbent.

2.4.1. Adsorption Kinetics

The experimental data were fitted by pseudo first order (PFO), pseudo second order (PSO), and intraparticle diffusion (ID) kinetic models, given by Equations (2), (3) and (4), respectively [36–39]:

$$q_t = q_e\left(1 - \exp^{-k_1 t}\right) \quad (2)$$

$$q_t = \frac{q_e^2 k_2 t}{q_e k_2 t + 1} \quad (3)$$

$$q_t = k_{ID} t^{0.5} + C \quad (4)$$

where q_t is the amount of phosphate (μmol) adsorbed per gram of adsorbent at time t, q_e is the fitted amount of phosphate adsorbed at the equilibrium (μmol g^{-1}), and k_1, k_2, and k_{ID} are the pseudo first order, pseudo second order, and intraparticle diffusion rate constants, respectively. The term C (Equation (4)) is related to the thickness of the boundary layer.

2.4.2. Adsorption Isotherms

The values of q versus c_P data were fitted to the Langmuir (one-site and two-site) and Freundlich equations (Equations (5), (6), and (8), respectively) [37].

$$q = q_{max} \frac{K_L c_P}{1 + K_L c_P} \tag{5}$$

$$q = q_{max,1} \frac{K_{L,1} c_P}{1 + K_{L,1} c_P} + q_{max,2} \frac{K_{L,2} c_P}{1 + K_{L,2} c_P} \tag{6}$$

where q_{max} is the maximum amount of phosphate adsorbed per unit mass of FeOH-Vt (μmol g^{-1}), and K_L is the Langmuir adsorption constant (L μmol^{-1}). In Equation (6), the indexes 1 and 2 correspond to sites 1 and 2, respectively.

From the K_L, it is possible to calculate the dimensionless constant separation factor (R_L) using Equation (7):

$$R_L = \frac{1}{1 + K_L C_0} \tag{7}$$

where C_0 is the largest initial concentration of adsorbate used in the adsorption isotherm (in μmol L^{-1}). If $0 < R_L < 1$, the adsorption is considered favorable, if $R_L > 1$ the adsorption is unfavorable and if $R_L = 0$ the adsorption is irreversible [40].

The Freundlich equation is represented by:

$$q = K_f c_P^{1/n} \tag{8}$$

where K_f is the Freundlich empirical constant related to adsorption capacity ($\mu mol^{1-1/n}\, g^{-1}\, L^{1/n}$), and 1/n is the nonlinearity parameter associated with the energetic heterogeneity of the adsorption sites.

2.4.3. Data Fitting

All fittings were made using the Origin 2020 64-bit Academic software (OriginLab Corporation, Northampton, MA, USA). While the one-site Langmuir and Freundlich equations were in the library of equations as Power Origin Functions, the code of the two-site model was quickly added to the equations library. Fittings were made using the Levenberger–Marquardt iteration algorithm. The maximum number of iterations and tolerance were 400 and 1×10^{-9} as the software's default. The fitting quality was tested by calculating the coefficient of determination (R^2, Equation (9)) and the chi-squared parameter (χ^2) (Equation (10)).

$$R^2 = 1 - \frac{\sum \left(q_{e,exp} - q_{e.calc} \right)^2}{\sum \left(q_{e,exp} - q_{e,mean} \right)^2} \tag{9}$$

$$\chi^2 = \sum \frac{\left(q_{e,exp} - q_{e,calc} \right)^2}{q_{e,calc}} \tag{10}$$

where $q_{e,exp}$ is the experimental value of q, measured at equilibrium, $q_{e,calc}$ is the fitted value of q, and $q_{e,mean}$ is the mean value of experimental q. The closer R^2 is to the 1, the better the fitting quality. In Equation (10), if $q_{e,calc}$ using a model is similar to the $q_{e,exp}$, χ^2 is close to zero. High χ^2 values indicate high bias between the experimental data and the tested model.

3. Results

3.1. Characterization of Na-Vt and FeOH-Vt

The CEC of Na-Vt was 1.154 ± 0.006 mmol g^{-1} (115.4 $cmol_c$ kg^{-1}), a value consistent with the CEC of other vermiculites (80 and 126 $cmol_c$ kg^{-1}) determined by the Cd^{2+} exchange method [24]. The iron content of the FeOH-VT was 1.208 mmol g^{-1}, as described by Nascimento and Masini [21]. This value approaches the CEC, suggesting the Fe^{3+} polyhydroxy cations quantitatively exchanged the Na^+ in the modification process. The incorporation of Fe^{3+} polycations changed the adsorbent color from gray to golden brown (Figure 1).

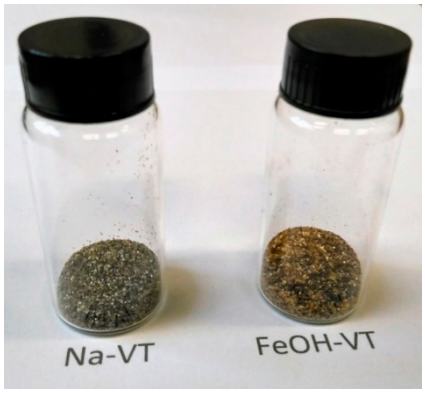

Figure 1. View of the gray Na-Vt compared to the golden brown modified FeOH-Vt.

The X-ray diffractometry of Na-Vt exhibits the typical peak at 2theta = 6.24° relative to the basal spacing (d001) of 1.415 nm (Figure 2), characteristic of hydrated vermiculites exchanged with Na^+. Other typical 2theta reflections appear at 24.16° and 30.28°, in agreement with Marcos et al. [41]. Other reflections at 2theta = 7.40°, 7.94° may be assigned to interlayered biotite [24], whereas reflections at 28.28° and 29.28° are due to unknown impurities. The exchange of Na^+ by Fe^{3+} polyhydroxy cations did not promote any significant alteration in the d001 basal space of the modified vermiculite (Figure 2). Similarly, the total surface area determined by the EGME method did not suffer significant alterations (122 ± 12 m^2 g^{-1} for FeOH-Vt and 112 ± 3 m^2 g^{-1} for Na-Vt) [21,31].

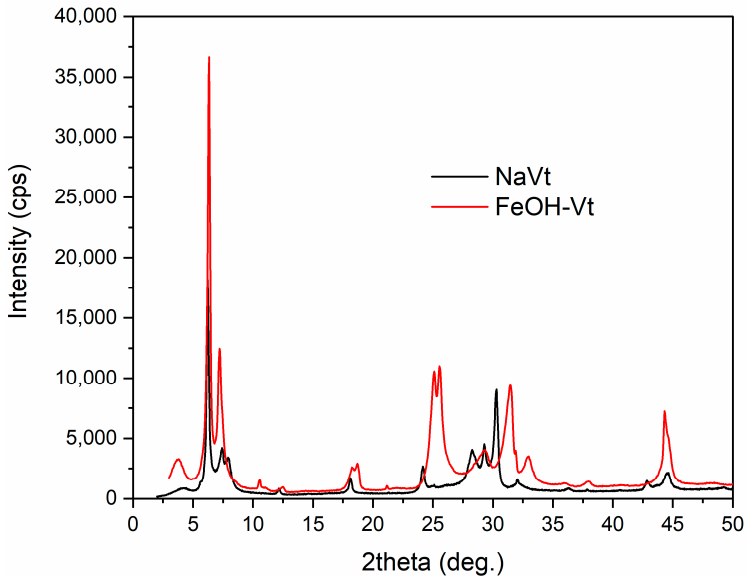

Figure 2. XRD patterns show the intense peak at 2θ = 6.24° for Na-Vt and 6.35° for FeOH-Vt, corresponding to the basal spacing of 1.415 and 1.390 nm, respectively.

Scanning electron microscopy images of both Na-Vt and FeOH-Vt (Figure 3) show the typical lamellar structures of vermiculites but without a significant morphological alteration after the intercalation of Fe^{3+} polyhydroxy cations (Figure 3).

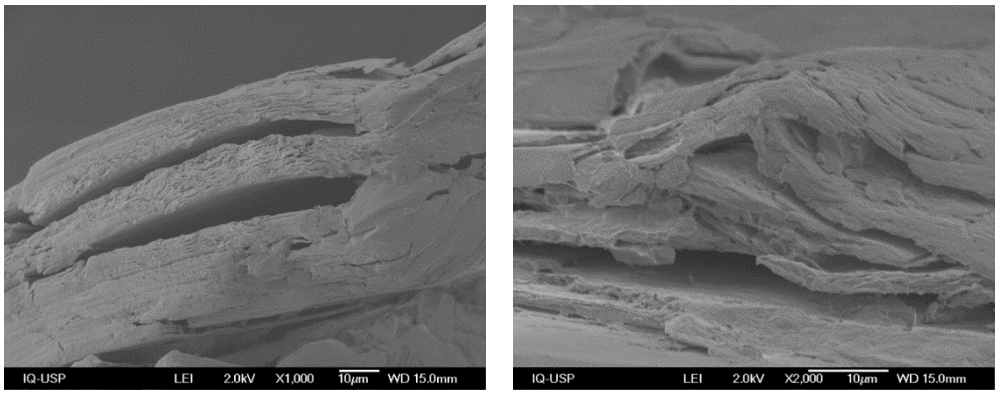

(**a**) (**b**)

Figure 3. Scanning electron microscopy of (**a**) Na-Vt and (**b**) FeOH-Vt.

3.2. Dose Effect

Initial exploratory experiments demonstrated that the adsorption onto NaVt was negligible, so the following parts of the article discuss only the adsorption on FeOH-Vt. The insignificant adsorption on NaVt may be explained by the high solubility of Na^+ phosphate salts, contrary to Fe^{3+}, which is known to form insoluble $FePO_4$. Furthermore, the Fe^{3+} polyhydroxy cations prepared with equimolar amounts of Fe^{3+} and OH^- have an excess of two positive charges per mole of polycations. Thus, electrostatic interaction is a possible retention mechanism in FeOH-Vt that is not likely to occur in NaVt.

The effect of the adsorbent dose for a contact time of 200 min (Figure 4) showed that the amount of phosphate adsorbed per unit of mass increased up to 75 mg of FeOH-Vt, but decreased as the adsorbent mass increased to 100 mg. The same initial amount of phosphate (3.77 μmol, or 0.15 mg of P) distributed in a larger adsorbent mass explains the drop of q as the mass increased from 75 to 100 mg. On the other hand, the absolute amount of phosphate, or the adsorption percentage, continuously increases with the FeOH-Vt mass (Figure 4). Thus, the adsorption kinetics and isotherms were investigated using 100 mg of FeOH-Vt dispersed in 10 mL of phosphate solution.

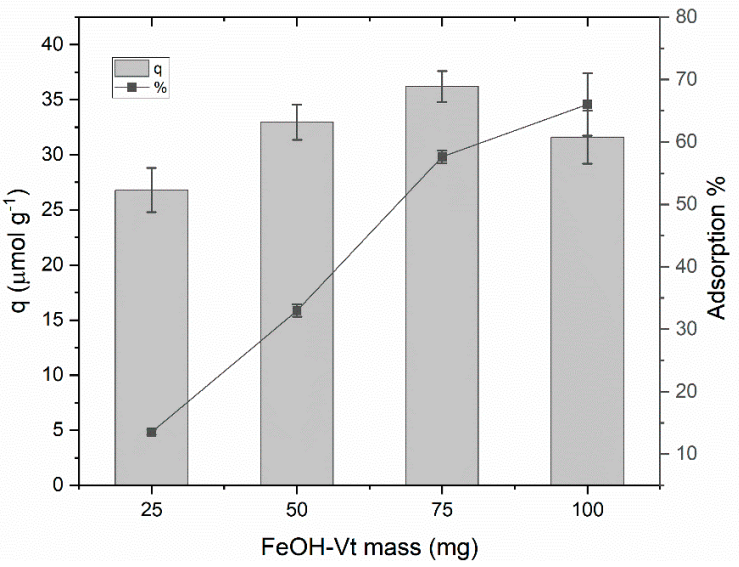

Figure 4. Dose effect investigation adopting a contact time of 200 min, initial phosphate concentration of 4.84×10^2 μmol L^{-1} (15 mg L^{-1} in P) and 25.0 ± 0.5 °C.

3.3. Adsorption Kinetics

The contact time of up 300–350 min removes about 90% of the phosphate from 10.0 mL of a 4.84 × 10^2 µmol L^{-1} phosphate solution (15.0 mg L^{-1} in P), dispersing 100 mg of FeOH-Vt (Figure 5) when the system approaches the equilibrium.

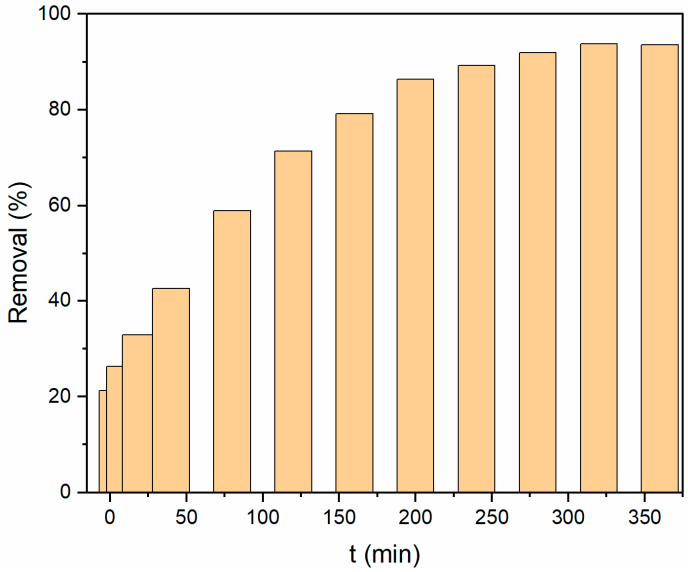

Figure 5. Adsorption percentages increase with time in a dispersion of 2.0 g of FeOH-Vt in 200 mL of an initial 4.84 × 10^2 µmol L^{-1} phosphate solution (15.0 mg L^{-1} in P).

Fitting the experimental data with the PFO, PSO and ID models (Figure 6) reveals that the PSO model provides slightly better R^2 and χ^2 values than those found from PFO (Table 1). The q_e was consistent in both models, at around 40–50 µmol g^{-1} (Table 1). However, the kinetics limiting factor is the intraparticle diffusion (inset in Figure 6) since the plot of q_t versus $t^{0.5}$ goes through the origin and has an excellent linear correlation coefficient (R^2 = 0.998, Table 1), consistent with the incorporation of Fe^{3+} polyhydroxy cations in the interlamellar space of vermiculite.

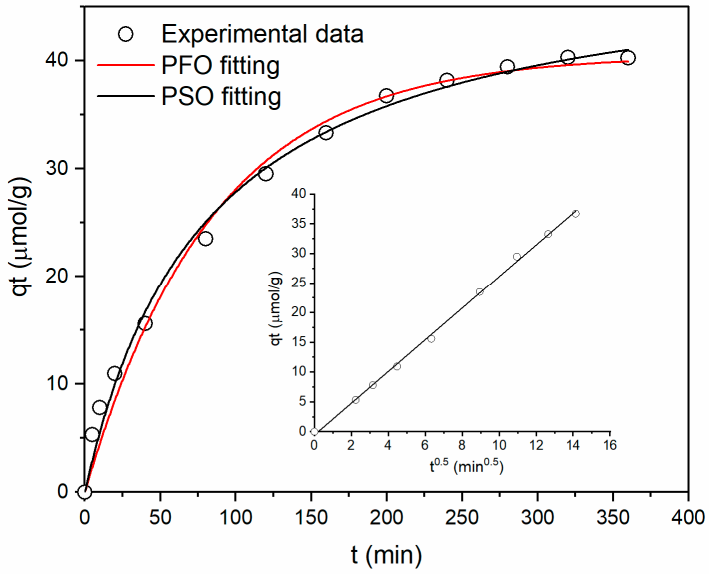

Figure 6. Adsorption kinetics in a dispersion of 2.0 g of FeOH-Vt in 200 mL of an initial 4.84 × 10^2 µmol L^{-1} phosphate solution (15.0 mg L^{-1} in P) fitted to the PFO and PSO kinetic models. The inset shows the data fitting to the ID model.

Table 1. Kinetic parameters fitted by PFO, PSO and ID models by NLR analysis.

Parameter	PFO	PSO	I.D.
q_e (μmol g^{-1})	40 ± 1	50 ± 2	-
$k^{1,2}$	0.012 ± 0.001	(2.4 ± 0.3) × 10^{-4}	-
$k_{I.D.}$ (μmol g^{-1} $min^{1/2}$)	-	-	2.67 ± 0.04
C (μmol g^{-1})	-	-	0.54 ± 0.32
R^2	0.987	0.992	0.998
χ^2	2.80	1.60	-

Units for PFO and PSO models are min^{-1} and g min μmol^{-1}, respectively.

3.4. Adsorption Isotherm

Adsorption isotherm data were fitted by Langmuir (one- and two-site) and Freundlich models (Figure 7). The Freundlich and two-site Langmuir models fitted the data much better than the one-site Langmuir model, as can be noticed by the R^2, which is much closer to the unity, and the smaller values of χ^2 (Table 2). The maximum adsorption capacity ($q_{max,1}$ + $q_{max,2}$ = 299 ± 69 μmol g^{-1}, or 9.3 ± 2.1 mg P g^{-1}) is comparable with several other phosphate adsorbents described in the literature, as will be discussed in the next section of this paper.

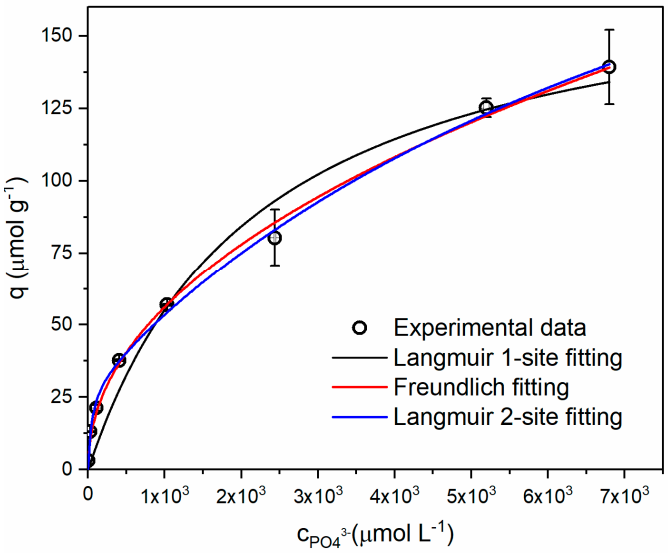

Figure 7. Adsorption isotherms (25.0 ± 0.5 °C) in dispersions of 100 mg of FeOH-Vt in 10 mL phosphate solution fitted to Langmuir (one- and two-site) and Freundlich.

Table 2. Adsorption isotherm (25.0 ± 0.5 °C) fitted by NLR analysis.

Isotherm Parameter	Langmuir One-Site	Langmuir Two-Site	Freundlich
$q_{max,1}$ (μmol g^{-1})	178 ± 24	30 ± 6	-
$q_{max,2}$ (μmol g^{-1})	-	269 ± 63	-
$K_{L,1}$ (L g^{-1})	(5 ± 2) × 10^{-4}	0.02 ± 0.01	-
$K_{L,2}$ (L g^{-1})	-	(1.0 ± 0.5) × 10^{-4}	-
K_F (μmol$^{1-1/n}$ g^{-1} $L^{1/n}$)	-	-	2.1 ± 0.3
1/n	-	-	0.47 ± 0.02
R^2	0.95	0.998	0.996
χ^2	116	9.66	9.62

The dimensionless separation factor R_L, computed for a C_0 = 8.07 × 10^3 μmol L^{-1}, was between 0.15 and 0.29, assuming the one-site Langmuir model, thus implying favorable adsorption. For the two-site model, the R_L values were between 0.0041 and 0.012, indicating

irreversible adsorption on site 1, whereas for site 2, the R_L was within the 0.45–0.71 range, thus indicating favorable adsorption.

4. Discussion

FeOH-Vt adsorbed phosphate from an aqueous medium with a performance similar to other adsorbents already described. For instance, the equilibrium approached with a contact time of about 200 min, corresponded with a similar condition reported for Phoslock™ [5], which required three hours of contact time. Other adsorbents such as Al/Fe-substituted bentonite required much more time (about nine hours) [42]. Other bentonite-based adsorbents prepared with La^{3+}/Al^{3+} or La^{3+}/Fe^{3+} substitutions required from 12 [43] to 96 h [11] to approach equilibrium. Several modified bentonites reached equilibrium within 24 h of contact time [44–48]. Few studies used vermiculite, but Huang et al. investigated the adsorption of phosphate on $La(OH)_3$-modified exfoliated vermiculite, finding an equilibrium with about 48 h of contact time [47].

Our research group recently modified commercial K10 montmorillonite with Fe^{3+} polyhydroxy cations prepared with different $Fe:OH^-$ molar ratios, including the 1:1 ratio used to modify Vt [19]. We named that material Mt-OH/$Fe_{1:1}$ and studied the phosphate adsorption under the same experimental conditions used for FeOH-Vt. Compared to the modified acid-activated K10 montmorillonite, the FeOH-Vt exhibited lower rate constants (0.012 ± 0.001 against 0.12 ± 0.01 min^{-1} in the PFO model, and $(2.4 \pm 0.3) \times 10^{-4}$ against 0.010 ± 0.001 g min μmol^{-1} for the PSO model). The faster adsorption onto Mt-OH/$Fe_{1:1}$ may be explained by the acid activation process that delaminates the structure and dissolves individual platelets leading to the formation of a low crystallinity, highly porous hydrated phase [49]. Thus, the phosphate adsorption on Mt-OH/$Fe_{1:1}$ is predominantly an external surface process, corroborated by applying the ID model (Equation (4)), which resulted in a C term of 24 ± 1 μmol g^{-1}, close to the q_e values fitted by nonlinear regression (around 28 μmol g^{-1}) [19]. In contrast with the Mt-OH/$Fe_{1:1}$, the ID model applied to the adsorption on FeOH-Vt resulted in a C value indistinguishable from zero (Table 1) and an excellent linear fitting in the time window between 0 and 180 min, thus suggesting that the modification of Vt occurred in the interlayers, and the pore diffusion became the rate-limiting step controlling the adsorption.

A one-site Langmuir model poorly fitted the adsorption isotherms, but the fitting was much improved using the Freundlich equation or the two-site Langmuir model. This finding is consistent with adsorption onto heterogeneous adsorbents, as corroborated by the 1/n Freundlich parameter of 0.47 ± 0.02 and the presence of adsorption sites with diverse adsorption strengths suggested by the excellent fitting to the two-site Langmuir model. The total adsorption capacity is 299 ± 69 μmol g^{-1}, which is similar to the results reported for Phoslock™ and several other adsorbents such as Fe/Zennith bentonite (360 μmol g^{-1} [5]), Al/Fe bentonite (181–364 μmol g^{-1} [42]), La/Al Mt (332–420 μmol g^{-1} [43]), and La/Fe Mt (30.1–188 μmol g^{-1} [11]), but being prepared with low-cost Fe^{3+} salts, rather than La^{3+} compounds, it is much more expensive, especially considering the use in large scale.

The q_{max} for FeOH-Vt is smaller than that found for Zr-modified bentonite (292.5–432.6 μmol g^{-1} [50]) and Zr/Al bentonite (555 μmol g^{-1} [48] and significantly lower than that observed for $La(OH)_3$-modified exfoliated vermiculite (2.57×10^3 μmol g^{-1} [47]). The increased adsorption capacity of Zr-modified bentonites may be related to the tetravalent nature of the cation and thus a more significant positive charge density on the external surface and an increase in the basal space, pore volume, and specific surface area compared to the unmodified Mt [48]. Regarding $La(OH)_3$-modified exfoliated vermiculite, the impressive increase in q_{max} may be related to the increase in specific surface area, pore volume, and pore diameter [47], which were not evidenced in the FeOH-Vt material compared to unmodified Na-Vt.

Compared with Mt-OH/$Fe_{1:1}$ under the same experimental conditions, the q_{max} of FeOH-Vt is significantly higher (299 ± 69 against 69 ± 3 μmol g^{-1}). The higher q_{max} strongly correlates with the iron content in the FeOH-Vt (1.208 mmol g^{-1}) compared to that

of Mt-OH/$Fe_{1:1}$ (0.57 ± 0.03 μmol g^{-1}) [19], providing a greater abundance of adsorption sites to interact with phosphate ions via the precipitation of isolube iron-phosphate salts, or electrostatic interactions with the exceeding positive charges of the polycations.

The separation factor (R_L) determined from the one-site Langmuir K_L ($0.15 < R_L < 0.29$) indicates that the adsorption is favorable. Regarding the two-site model, a similar finding comes from the R_L between 0.45 and 0.71 obtained for site 2, which is more abundant, but has a low K_L, that is, a low energy process, while for site 1, the R_L was in the 0.0041 to 0.012 range, indicating an irreversible process in a highly energetic interaction with sites of low abundance. Thus, whereas the adsorption is favorable in all the studied phosphate concentration ranges, the adsorption is irreversible under the lower concentrations interacting with site 1. This heterogeneity of adsorption sites is consistent with the excellent fitting obtained with the Freundlich equation, especially with the 1/n value of 0.47 ± 0.02, characteristic of highly heterogeneous adsorption processes [37,51].

FeOH-Vt was then applied to a water sample collected at the Guarapiranga Reservoir, which plays an essential role as a water supply to about four million people in the Metropolitan Area of São Paulo city, Brazil. Although subject to the diffuse discharge of municipal waste, no phosphate was quantifiable by the spectrophotometric blue molybdenum method (LOQ = 2.0 μmol L^{-1}, or 0.063 mg L^{-1} in P). Thus, the sample was spiked with 251 μmol L^{-1} phosphate (10 mg L^{-1} in P) and exposed to FeOH-Vt under constant stirring for 200 min. After this contact time, the remaining phosphate concentration was 72.3 μmol L^{-1} (2.9 mg L^{-1} in P), implying about 71% removal.

5. Conclusions

Modifying vermiculite with Fe^{3+} polyhydroxy cations enhanced the capacity and affinity of the obtained FeOH-Vt compared to the unmodified clay mineral for phosphate removal. The modification is simple, using low-cost, environmentally compatible Fe^{3+} salts. Phosphate adsorption was fast compared to other adsorbents and limited mainly by intraparticle diffusion. The adsorption was favorable, exhibiting irreversible interaction in a small fraction of the adsorption sites as suggested by fitting the data to the two-site Langmuir isotherm.

Supplementary Materials: The following are available online at https://www.mdpi.com/article/10.3390/min12081033/s1, Table S1: Effect of mass of FeOH-Vt on the adsorption of Phosphate from a 15.0 mg L^{-1} (in P) after 200 min of contact time under stirring. Temperature = 25.0 ± 0.5 °C, Table S2: Adsorption kinetics data obtained in a dispersion of 2.0 g of FeOH-Vt in 200 mL of an initial 4.84×10^2 μmol L^{-1} phosphate solution (15.0 mg L^{-1} in P), Table S3: Data of adsorption isotherms (25.0 ± 0.5 °C) in dispersions of 100 mg of FeOH-Vt in 10 mL phosphate solution with initial concentrations between 1.0 and 250.0 mg L^{-1} in P.

Author Contributions: Conceptualization, J.C.M. and F.H.d.N.; methodology, F.H.d.N.; validation, J.C.M., F.H.d.N.; formal analysis, J.C.M., F.H.d.N.; investigation, F.H.d.N.; resources, J.C.M.; writing—original draft preparation, F.H.d.N.; writing—review and editing, J.C.M.; supervision, J.C.M.; funding acquisition, J.C.M. All authors have read and agreed to the published version of the manuscript.

Funding: This research was funded by National Council for Scientific and Technological Development (CNPq), grant number 306674/2021-1. Fernando H. do Nascimento acknowledges Coordination for the Improvement of Higher Education Personnel (CAPES) for a post-doc fellowship (Contract 88882.315696/2019-01).

Data Availability Statement: The data presented in this study are available in the supplementary material.

Conflicts of Interest: The authors declare no conflict of interest.

References

1. Cunha, D.G.F.; Casali, S.P.; de Falco, P.B.; Thornhill, I.; Loiselle, S.A. The Contribution of Volunteer-Based Monitoring Data to the Assessment of Harmful Phytoplankton Blooms in Brazilian Urban Streams. *Sci. Total Environ.* **2017**, *584–585*, 586–594. [CrossRef] [PubMed]
2. Abukhadra, M.R.; Adlii, A.; El-Sherbeeny, A.M.; Ahmed Soliman, A.T.; Abd Elgawad, A.E.E. Promoting the Decontamination of Different Types of Water Pollutants (Cd^{2+}, Safranin Dye, and Phosphate) Using a Novel Structure of Exfoliated Bentonite Admixed with Cellulose Nanofiber. *J. Environ. Manag.* **2020**, *273*, 111130. [CrossRef] [PubMed]
3. Zamparas, M.; Drosos, M.; Georgiou, Y.; Deligiannakis, Y.; Zacharias, I. A Novel Bentonite-Humic Acid Composite Material Bephos^{TM} for Removal of Phosphate and Ammonium from Eutrophic Waters. *Chem. Eng. J.* **2013**, *225*, 43–51. [CrossRef]
4. Zamparas, M.; Drosos, M.; Kalavrouziotis, I.K. Sorption of Phosphate from Innovative Composite Material Focusing on Physicochemical Interactions. *Desalin. Water Treat.* **2019**, *151*, 212–218. [CrossRef]
5. Zamparas, M.; Gianni, A.; Stathi, P.; Deligiannakis, Y.; Zacharias, I. Removal of Phosphate from Natural Waters Using Innovative Modified Bentonites. *Appl. Clay Sci.* **2012**, *62–63*, 101–106. [CrossRef]
6. Zhang, Y.; Pan, B.; Shan, C.; Gao, X. Enhanced Phosphate Removal by Nanosized Hydrated La(III) Oxide Confined in Cross-Linked Polystyrene Networks. *Environ. Sci. Technol.* **2016**, *50*, 1447–1454. [CrossRef]
7. Kurzbaum, E.; Bar Shalom, O. The Potential of Phosphate Removal from Dairy Wastewater and Municipal Wastewater Effluents Using a Lanthanum-Modified Bentonite. *Appl. Clay Sci.* **2016**, *123*, 182–186. [CrossRef]
8. Li, J.R.; Xu, L.; He, M.M.; Xiao, H. Enhancement of Kaolin Adsorption Affinity Toward Phosphate by Sequestrating Naturally Abundant Ca/Mg From Seawater. *Clean Soil Air Water* **2018**, *46*. [CrossRef]
9. Li, J.R.; Zhu, L.; Tang, J.; Qin, K.; Li, G.; Wang, T.H. Sequestration of Naturally Abundant Seawater Calcium and Magnesium to Enhance the Adsorption Capacity of Bentonite toward Environmental Phosphate. *RSC Adv.* **2016**, *6*, 23252–23259. [CrossRef]
10. An, X.; Wu, Z.; Yu, J.; Ge, L.; Li, T.; Liu, X.; Yu, B. High-Efficiency Reclaiming Phosphate from an Aqueous Solution by Bentonite Modified Biochars: A Slow Release Fertilizer with a Precise Rate Regulation. *ACS Sustain. Chem. Eng.* **2020**, *8*, 6090–6099. [CrossRef]
11. de Castro, L.; Brandão, V.; Bertolino, L.; de Souza, W.; Teixeira, V. Phosphate Adsorption by Montmorillonites Modified with Lanthanum/Iron and a Laboratory Test Using Water from the Jacarepaguá Lagoon (RJ, Brazil). *J. Braz. Chem. Soc.* **2018**, *30*, 641–657. [CrossRef]
12. Zamparas, M.; Deligiannakis, Y.; Zacharias, I. Phosphate Adsorption from Natural Waters and Evaluation of Sediment Capping Using Modified Clays. *Desalin. Water Treat.* **2013**, *51*, 2895–2902. [CrossRef]
13. El Bouraie, M.; Masoud, A.A. Adsorption of Phosphate Ions from Aqueous Solution by Modified Bentonite with Magnesium Hydroxide $Mg(OH)_2$. *Appl. Clay Sci.* **2017**, *140*, 157–164. [CrossRef]
14. Kong, L.; Tian, Y.; Li, N.; Liu, Y.; Zhang, J.; Zhang, J.; Zuo, W. Highly-Effective Phosphate Removal from Aqueous Solutions by Calcined Nano-Porous Palygorskite Matrix with Embedded Lanthanum Hydroxide. *Appl. Clay Sci.* **2018**, *162*, 507–517. [CrossRef]
15. Kuroki, V.; Bosco, G.E.; Fadini, P.S.; Mozeto, A.A.; Cestari, A.R.; Carvalho, W.A. Use of a La(III)-Modified Bentonite for Effective Phosphate Removal from Aqueous Media. *J. Hazard. Mater.* **2014**, *274*, 124–131. [CrossRef]
16. dos Anjos, V.E.; Rohwedder, J.R.; Cadore, S.; Abate, G.; Grassi, M.T. Montmorillonite and Vermiculite as Solid Phases for the Preconcentration of Trace Elements in Natural Waters: Adsorption and Desorption Studies of As, Ba, Cu, Cd, Co, Cr, Mn, Ni, Pb, Sr, V, and Zn. *Appl. Clay Sci.* **2014**, *99*, 289–296. [CrossRef]
17. Abollino, O.; Giacomino, A.; Malandrino, M.; Mentasti, E. Interaction of Metal Ions with Montmorillonite and Vermiculite. *Appl. Clay Sci.* **2008**, *38*, 227–236. [CrossRef]
18. Huo, J.; Min, X.; Wang, Y. Zirconium-Modified Natural Clays for Phosphate Removal: Effect of Clay Minerals. *Environ. Res.* **2021**, *194*, 110685. [CrossRef]
19. Leite, S.T.; do Nascimento, F.H.; Masini, J.C. Fe(III)-Polyhydroxy Cations Supported onto K10 Montmorillonite for Removal of Phosphate from Waters. *Heliyon* **2020**, *6*, e03868. [CrossRef]
20. Baigorria, E.; Cano, L.; Sapag, K.; Alvarez, V. Removal Efficiency of As(III) from Aqueous Solutions Using Natural and Fe(III) Modified Bentonites. *Environ. Technol.* **2021**, 1–14. [CrossRef]
21. Nascimento, F.H.D.; Masini, J.C. An Electrochemical Sequential Injection Method to Investigate the Adsorption of Selenite on Fe(III) Polyhydroxy Cations Intercalated Vermiculite. *Water Sci. Technol.* **2018**, *2017*, 134–143. [CrossRef] [PubMed]
22. Bleam, W. Clay Mineralogy and Chemistry. In *Soil and Environmental Chemistry*; Academic Press: Cambridge, MA, USA, 2017; pp. 87–146; ISBN 9780128041789.
23. Abate, G.; Lichtig, J.; Masini, J.C. Construction and Evaluation of a Flow-through Cell Adapted to a Commercial Static Mercury Drop Electrode (SMDE) to Study the Adsorption of Cd(II) and Pb(II) on Vermiculite. *Talanta* **2002**, *58*, 433–443. [CrossRef]
24. Valášková, M.; Kupková, J.; Martynková, G.S.; Seidlerová, J.; Tomášek, V.; Ritz, M.; Kočí, K.; Klemm, V.; Rafaja, D. Comparable Study of Vermiculites from Four Commercial Deposits Prepared with Fixed Ceria Nanoparticles. *Appl. Clay Sci.* **2018**, *151*, 164–174. [CrossRef]
25. Abate, G.; Masini, J.C. Influence of pH, Ionic Strength and Humic Acid on Adsorption of Cd(II) and Pb(II) onto Vermiculite. *Colloids Surfaces A Physicochem. Eng. Asp.* **2005**, *262*, 33–39. [CrossRef]

26. Macht, F.; Eusterhues, K.; Pronk, G.J.; Totsche, K.U. Specific Surface Area of Clay Minerals: Comparison between Atomic Force Microscopy Measurements and Bulk-Gas (N2) and -Liquid (EGME) Adsorption Methods. *Appl. Clay Sci.* **2011**, *53*, 20–26. [CrossRef]
27. Zarpon, L.; Abate, G.; do Santos, L.B.O.; Masini, J.C. Montmorillonite as an Adsorbent for Extraction and Concentration of Atrazine, Propazine, Deethylatrazine, Deisopropylatrazine and Hydroxyatrazine. *Anal. Chim. Acta* **2006**, *579*, 81–87. [CrossRef] [PubMed]
28. Vieira dos Santos, A.C.; Masini, J.C. Evaluating the Removal of Cd(II), Pb(II) and Cu(II) from a Wastewater Sample of a Coating Industry by Adsorption onto Vermiculite. *Appl. Clay Sci.* **2007**, *37*, 167–174. [CrossRef]
29. Infante, C.M.C.; Masini, J.C. Development of a Spectrophotometric Sequential Injection Methodology for Online Monitoring of the Adsorption of Paraquat on Clay Mineral and Soil. *Spectrosc. Lett.* **2007**, *40*, 3–14. [CrossRef]
30. Abate, G.; Masini, J.C. Adsorption of Atrazine, Hydroxyatrazine, Deethylatrazine, and Deisopropylatrazine onto Fe(III) Polyhydroxy Cations Intercalated Vermiculite and Montmorillonite. *J. Agric. Food Chem.* **2005**, *53*, 1612–1619. [CrossRef]
31. Do Nascimento, F.H.; de Souza Costa, D.M.; Masini, J.C. Evaluation of Thiol-Modified Vermiculite for Removal of Hg(II) from Aqueous Solutions. *Appl. Clay Sci.* **2016**, *124–125*, 227–235. [CrossRef]
32. Abate, G.; Masini, J.C. Influence of PH and Ionic Strength on Removal Processes of a Sedimentary Humic Acid in a Suspension of Vermiculite. *Colloids Surfaces A Physicochem. Eng. Asp.* **2003**, *226*, 25–34. [CrossRef]
33. Marcos, C.; Rodríguez, I.; Clauzio De Rennó, L.; Paredes, G.J. Vermiculite Surface Structure as Imaged by Contact Mode AFM. *Eur. J. Mineral.* **2004**, *16*, 597–607. [CrossRef]
34. Hesse, P.R. *A Textbook of Soil Chemical Analysis*; John Murray Publishers: London, UK, 1971.
35. Galhardo, C.X.; Masini, J.C. Spectrophotometric Determination of Phosphate and Silicate by Sequential Injection Using Molybdenum Blue Chemistry. *Anal. Chim. Acta* **2000**, *417*, 191–200. [CrossRef]
36. Lagergren, S. About the Theory of So-Called Adsorption of Soluble Substances. *K. Sven. Vetensk. Handl.* **1898**, *24*, 1–39.
37. Tran, H.N.; You, S.J.; Hosseini-Bandegharaei, A.; Chao, H.P. Mistakes and Inconsistencies Regarding Adsorption of Contaminants from Aqueous Solutions: A Critical Review. *Water Res.* **2017**, *120*, 88–116. [CrossRef]
38. Blanchard, G.; Maunaye, M.; Martin, G. Removal of Heavy Metals from Waters by Means of Natural Zeolites. *Water Res.* **1984**, *18*, 1501–1507. [CrossRef]
39. Weber, W.J.; Morris, J.C. Kinetics of Adsorption on Carbon from Solutions. *J. Sanit. Eng. Div.* **1963**, *89*, 31–59. [CrossRef]
40. Hall, K.R.; Eagleton, L.C.; Acrivos, A.; Vermeulen, T. Pore- and Solid-Diffusion Kinetics in Fixed-Bed Adsorption under Constant-Pattern Conditions. *Ind. Eng. Chem. Fundam.* **1966**, *5*, 212–223. [CrossRef]
41. Marcos, C.; Arango, Y.C.; Rodriguez, I. X-Ray Diffraction Studies of the Thermal Behaviour of Commercial Vermiculites. *Appl. Clay Sci.* **2009**, *42*, 368–378. [CrossRef]
42. Shanableh, A.; Enshasi, G.; Elsergany, M. Phosphorous Adsorption Using Al^{3+}/Fe^{3+}-Modified Bentonite Adsorbents—Effect of Al^{3+} and Fe^{3+} Combinations. *Desalin. Water Treat.* **2016**, *57*, 15628–15634. [CrossRef]
43. Tian, S.; Jiang, P.; Ning, P.; Su, Y. Enhanced Adsorption Removal of Phosphate from Water by Mixed Lanthanum/Aluminum Pillared Montmorillonite. *Chem. Eng. J.* **2009**, *151*, 141–148. [CrossRef]
44. Wang, Y.; He, H.; Zhang, N.; Shimizu, K.; Lei, Z.; Zhang, Z. Efficient Capture of Phosphate from Aqueous Solution Using Acid Activated Akadama Clay and Mechanisms Analysis. *Water Sci. Technol.* **2018**, *78*, 1603–1614. [CrossRef] [PubMed]
45. Chen, X.; Wu, L.; Liu, F.; Luo, P.; Zhuang, X.; Wu, J.; Zhu, Z.; Xu, S.; Xie, G. Performance and Mechanisms of Thermally Treated Bentonite for Enhanced Phosphate Removal from Wastewater. *Environ. Sci. Pollut. Res.* **2018**, *25*, 15980–15989. [CrossRef] [PubMed]
46. Lin, J.; He, S.; Zhan, Y.; Zhang, H. Evaluation of Phosphate Adsorption on Zirconium/Magnesium-Modified Bentonite. *Environ. Technol.* **2020**, *41*, 586–602. [CrossRef]
47. Huang, W.Y.; Li, D.; Liu, Z.Q.; Tao, Q.; Zhu, Y.; Yang, J.; Zhang, Y.M. Kinetics, Isotherm, Thermodynamic, and Adsorption Mechanism Studies of $La(OH)_3$-Modified Exfoliated Vermiculites as Highly Efficient Phosphate Adsorbents. *Chem. Eng. J.* **2014**, *236*, 191–201. [CrossRef]
48. Huang, W.; Chen, J.; He, F.; Tang, J.; Li, D.; Zhu, Y.; Zhang, Y. Effective Phosphate Adsorption by Zr/Al-Pillared Montmorillonite: Insight into Equilibrium, Kinetics and Thermodynamics. *Appl. Clay Sci.* **2015**, *104*, 252–260. [CrossRef]
49. Wallis, P.J.; Gates, W.P.; Patti, A.F.; Scott, L.; Teoh, E. Cutting-Edge Research for a Greener Sustainable Future Assessing and Improving the Catalytic Activity of K-10 Montmorillonite. *Green Chem.* **2007**, *9*, 980–985. [CrossRef]
50. Lin, J.; Jiang, B.; Zhan, Y. Effect of Pre-Treatment of Bentonite with Sodium and Calcium Ions on Phosphate Adsorption onto Zirconium-Modified Bentonite. *J. Environ. Manag.* **2018**, *217*, 183–195. [CrossRef]
51. Masini, J.C.; Abate, G. Guidelines to Study the Adsorption of Pesticides onto Clay Minerals Aiming at a Straightforward Evaluation of Their Removal Performance. *Minerals* **2021**, *11*, 1282. [CrossRef]